

Graph Partial Label Learning with Potential Cause Discovering

Hang Gao^{1,2}, Jiaguo Yuan^{1,2}, Jiangmeng Li¹, Chengyu Yao^{1,2}, Fengge Wu^{1,2}, Junsuo Zhao¹ and Changwen Zheng^{*1,2}

¹ Institute of Software, Chinese Academy of Sciences

² University of Chinese Academy of Sciences

{hanggao,jiangmeng2019,fengge,junsuo,changwen}@iscas.ac.cn

{yuanjiaguo2022,yaochengyu2022}@mails.ucas.ac.cn

Abstract

Graph Neural Networks (GNNs) have gained considerable attention for their potential in addressing challenges posed by complex graph-structured data in diverse domains. However, accurately annotating graph data for training is difficult due to the inherent complexity and interconnectedness of graphs. To tackle this issue, we propose a novel graph representation learning method that enables GNN models to effectively learn discriminative information even in the presence of noisy labels within the context of Partially Labeled Learning (PLL). PLL is a critical weakly supervised learning problem, where each training instance is associated with a set of candidate labels, including both the true label and additional noisy labels. Our approach leverages potential cause extraction to obtain graph data that exhibit a higher likelihood of possessing a causal relationship with the labels. By incorporating auxiliary training based on the extracted graph data, our model can effectively filter out the noise contained in the labels. We support the rationale behind our approach with a series of theoretical analyses. Moreover, we conduct extensive evaluations and ablation studies on multiple datasets, demonstrating the superiority of our proposed method.

1 Introduction

Learning graph representations has emerged as a pivotal research area within the field of computer science, garnering significant attention from both academia and industry [Jiao *et al.*, 2023]. This burgeoning interest is primarily motivated by the pressing need to address the challenges posed by complex graph-structured data pervasive in diverse domains, such as social networks [Shen *et al.*, 2023], biological interactions [Zhang *et al.*, 2022], citation networks [Wang *et al.*, 2022b], and knowledge graphs [Shen *et al.*, 2023]. However, in the realm of graph representation learning, accurately annotating required training data has long been a challenging task, owing to the inherent complexity of the data [Pikhurko and Verbitsky, 2009]. Unlike traditional tabular data, graphs encompass

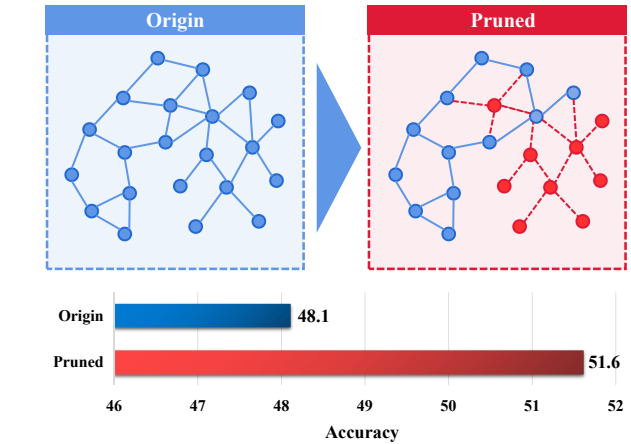


Figure 1: Compared results using ARMA. We conducted pruning on the training data and trained the identical model on both the original and pruned datasets separately. Subsequently, we assessed the models’ performance on the same test set to compare their effectiveness with distinct training data.

intricate relationships and interconnectedness between entities, rendering manual annotation laborious and error-prone [Shamsi *et al.*, 2022]. Though unsupervised methods [Xia *et al.*, 2021; You *et al.*, 2020] have shown promise in reducing reliance on annotated data to some extent in graph representation learning, they still fall short when it comes to handling the challenges posed by utilizing labeled data with noise. While some research efforts have attempted to address the issue of label noise, this direction of work remains an ongoing challenge with no definitive solution yet.

PLL [Szummer, 2002] is a weakly supervised learning task designed to handle scenarios where noise exists within the labels. In PLL, each training sample is associated with multiple labels, while only one of them is the ground truth label. Therefore, PLL allows for less-than-perfect accuracy during actual data annotation [Gong *et al.*, 2022]. In this study, we aim to address the aforementioned challenges by introducing PLL into the context of graph representation learning. However, the inherent structural complexity and semantically rich nature of graph data make the PLL problem in graph representation learning more challenging. But, recent advancements in graph causal learning have shown promising poten-

tial in reducing noise in data and revealing causal relationships [Wu *et al.*, 2022b; Fan *et al.*, 2022a]. Inspired by such approaches, we propose that leveraging causal reasoning allows for the partial removal of data in the graph that lacks causal relationships with the labels, resulting in a more refined graph data. When training with this refined data, the model can effectively mitigate the impact of noise in the labels, enabling better performance within the PLL scenario.

In order to validate our proposed approach, we conducted a motivational experiment based on baseline ARMA [Bianchi *et al.*, 2022]. In Figure 1, we applied a pruning based on Granger Causality [Dutta, 2001] to the graph data, aiming to retain nodes that exhibit causal relationships with the ground-truth labels and remove the remaining data. Subsequently, we trained the GNN model on this pruned dataset under the PLL scenario. We then compared the performance of this model with the model trained on the unpruned dataset under the same scenario. The results demonstrated that training on the pruned graph data led to superior performance. These experimental findings highlight the efficacy of extracting data that are causally related to the labels for graph learning in PLL scenarios. The underlying reason behind this discovery lies in the fact that extracting such data partially eliminates the interference of other noise present in the original graphs. Consequently, when utilizing GNN to model the statistical relationship between labels and data, it prevents the model from learning spurious correlations unrelated to the causal factors. Unfortunately, the aforementioned methods require a GNN model pre-trained on a noise-free dataset, rendering them inadequate for addressing our specific problem.

To identify graph data with causal relationships to ground-truth labels and enhance GNN model training in the context of PLL, we propose a novel approach named *Graph Potential Causes Discovering* (GPCD). To extract the desired data, we introduce the concept of potential causes from causal theory [Pearl and others, 2000]. Through theoretical validation, we demonstrate that identifying such causes can help pinpoint graph data exhibiting causal relationships with the ground-truth labels. In order to find the potential causes, we first employ a specialized model architecture to enable the identification of candidate causes. Subsequently, we refine and extract potential causes from these candidates. Utilizing the identified data, we model the relationship between the data and labels, guiding the model training process. Furthermore, we provide theoretical justification for our proposed design. In empirical evaluations, we comprehensively assess GPCD’s performance on seven different datasets, demonstrating its superiority over state-of-the-art methods in classification tasks.

Our contributions are summarized as follows:

- We propose an innovative method, GPCD, which optimizes graph representation learning under the PLL scenario by extracting potential causes. This approach offers a novel solution for effectively utilizing graph training data with noise in labels.
- We have conducted comprehensive theoretical analyses of GPCD. The utility of potential causes and the rationality of the potential cause extraction method have been rigorously proven and justified.

- We have provided a concrete implementation of GPCD and extensively evaluated its performance through a series of experiments. The results of these experiments, conducted on seven different datasets, demonstrate the superiority of the GPCD method.

2 Related Works

2.1 Causal Graph Learning

Currently, causal learning [Guo *et al.*, 2021] finds its application within graph learning paradigms, aiming to bolster interpretability and enhance models by discerning causal relationships existing between data and labels. This array of methodologies can be delineated into two fundamental strata: Inherent Interpretability and Invariant Learning. Approaches underpinned by inherent interpretability integrate rationalization modules, typified by mechanisms like attention [Velickovic *et al.*, 2017; Vaswani *et al.*, 2017] and pooling [Nguyen and Grishman, 2018; Lee *et al.*, 2019; Wu *et al.*, 2022a]. In contrast, methods predicated upon invariant learning are crafted to discern pivotal subgraphs that wield a determinative role in the prognostications of GNNs [Ying *et al.*, 2019; Chang *et al.*, 2020; Bevilacqua *et al.*, 2021]. Additionally, the paradigm of invariant learning finds utility in mitigating the challenges of generalization pertaining to out-of-distribution (OOD) data [Wu *et al.*, 2022b; Fan *et al.*, 2022a; Chen *et al.*, 2022]. We employ causal learning to aid us in combating noise present within the labels.

2.2 Partial Label Learning

Methods addressing the PLL problem mainly consist of two types: average-based methods and identification-based methods. The average-based method treats each label in the candidate label set equally, assigning equal weight to each label [Cour *et al.*, 2011; Hüllermeier and Beringer, 2006; Zhang and Yu, 2015]. The identification-based method treats the ground-truth label as a latent variable and identifies the ground-truth label iteratively during the learning process [Jin and Ghahramani, 2002; Liu and Dietterich, 2012; Nguyen and Caruana, 2008; Yu and Zhang, 2016; Chai *et al.*, 2019]. In addition, recently, confidence-based methods have achieved promising results. e.g., Pico [Wang *et al.*, 2022a] employs contrastive learning [He *et al.*, 2020] and class prototype-based label disambiguation to address PLL. We, on the other hand, aim to incorporate PLL into graph representation learning from a causal perspective.

3 Methodology

3.1 Preliminary

Partial Label Learning.

PLL investigates the challenge of learning from training sample X and its corresponding labels Y . The label Y comprises two components: the ground-truth label Y^* and irrelevant noisy label \tilde{Y} . If we denote \mathcal{Y} as the value space for labels, we have $Y^* \in \mathcal{Y}$ and $\tilde{Y} \in \mathcal{Y}$. Notably, Y^* and \tilde{Y} are indistinguishable directly. The primary objective of PLL is to train a model that can effectively capture the underlying relationship

between X and Y^* , even in the presence of interference from \tilde{Y} , and subsequently make accurate predictions.

Our focus lies in addressing the problem of PLL within the context of graph representation learning. Specifically, we endeavor to train a dedicated GNN denoted as $f(\cdot)$, employing graph data G and corresponding labels Y . The GNN model $f(\cdot)$ should possess the capability to predict Y^* based on the information in G .

Potential Cause.

In the domain of causality, the term ‘‘potential cause’’ refers to the variable X that could potentially exert a causal influence on another variable Y . In [Pearl and others, 2000], The Local Criteria for Inferring Causal Relations gives the precise definition and methods for determining potential causes:

Definition 1. (Potential Cause) [Pearl and others, 2000] A variable X has a potential causal influence on another variable Y if the following conditions hold.

1. X and Y are dependent in every context.
2. There exists a variable Z and a context S such that
 - (i) X and Z are independent given S and
 - (ii) Z and Y are dependent given S .

Within the definition, the term ‘‘context’’ means a set of variables tied to specific values. We employ this definition to aid in the identification of variables that can contribute positively to the learning process.

3.2 Learning Guided with Potential Causes Discovering

Theoretical Analysis.

We now proceed to introduce our proposed methodology. Firstly, in order to conduct a thorough analysis of the causal relationships and the PLL problem within the graph, we begin by providing a definition of causal redundancy in graph data.

Definition 2. (Causal Redundancy) Graph data G is considered to be ‘‘causally redundant’’ if there exists a non-empty subgraph $\tilde{G} \subset G$ such that the following condition holds:

$$f_{\theta^*}(G) = f_{\theta^*}(G \setminus \tilde{G}), \quad (1)$$

where $f_{\theta^*}(\cdot)$ represents a GNN that accurately captures the causal relationship between G and its corresponding ground truth label Y^* . The function $f_{\theta^*}(\cdot)$ is capable of providing correct predictions given any input. The symbol \setminus denotes the set difference operation.

Intuitively, by eliminating redundant information from G , we can obtain refined graph data denoted as G^* . We illustrate the existence of such refined representations, G^* , for each G through the following corollary.

Corollary 1. If G is causally redundant, then there exists a graph G^* that is part of G and is not causally redundant. Furthermore, G^* satisfies:

1. $f_{\theta^*}(G) = f_{\theta^*}(G^*)$.
2. $I(f_{\theta^*}(G^*); Y) > I(f_{\theta^*}(G^* \setminus \tilde{G}); Y), \forall \tilde{G} \subset G^* \text{ and } \tilde{G} \neq \emptyset$.

The proof can be found in **Appendix A.1**. Furthermore, as G^* only contains information relevant to the ground-truth label Y^* , it’s possible that by relying solely on G^* and Y — which includes both Y^* and the noisy label \tilde{Y} — one can still effectively model the causal relationships between G^* and Y^* . Specifically, considering a training set $\{G_i\}_{i=0}^N$ along with its corresponding labels $\{Y_i\}_{i=0}^N$, where $Y_i \in \mathbb{R}^{D \times K}$. Here, K represents the number of labels associated with each sample, and D denotes the number of classes. Y_i consist of Y_i^* and irrelevant noisy label \tilde{Y}_i , where Y_i^* is a single one-hot vector and \tilde{Y}_i can be either a single one-hot vector or multiple one-hot vectors. It is impossible to directly distinguish Y_i^* and \tilde{Y}_i in PLL scenarios.

Likewise, we denote G_i^* as a part within G that is not causally redundant. Furthermore, $G_i^* \in \mathcal{G}^*$, where \mathcal{G}^* denote the value space of all possible value of G^* . Within such a training set, we demonstrate the aforementioned intuition with the following theorem.

Theorem 1. Assuming that the noisy label \tilde{Y}_i within Y_i is not fully constrained by the information encapsulated in G_i^* and the ancestors of G_i^* , and contains single one-hot vector. Subsequently, we proceed to define a loss function as follows:

$$\mathcal{L} = \sum_{i=1}^N \sum_{k=1}^K \mathcal{H}\left(e^{(f_{\theta}(G_i^*))^\lambda}, Y_{i,k}\right), \lambda > 1, \quad (2)$$

where N is a sufficiently large number to ensure the dataset holds comprehensive coverage of values encompassed by \mathcal{G}^* . If \mathcal{L} attains its respective minimum value, then we can conclude that $f_{\theta}(G) = f_{\theta^*}(G)$.

The proof can be found in **Appendix A.2**. Theorem 1 demonstrates that finding G^* enables us to acquire a model that is equivalent to the desired GNN $f_{\theta^*}(\cdot)$ based on Y containing noisy labels. We can infer that under certain conditions, Theorem 1 remains valid in a more extensive range of scenarios. We demonstrate such inference with the following corollary.

Corollary 2. Theorem 1 will still hold for \tilde{Y}_i that consists of multiple one-hot vectors if the parameter λ in \mathcal{L} is large enough.

The proof and required values for the parameter λ can be found in **Appendix A.3**. However, finding G^* is a rather challenging task. Therefore, we incorporate the concept of potential causes from causality to approximate the identification of the elements present in G^* . We propose that finding the potential causes of Y can create an estimation of G^* . Subsequently, we provide a theoretical justification for the validity of such incorporation.

Theorem 2. If we denote the potential cause of Y as X_h and the set of all potential causes of Y as $\bigcap_{h \in H} X_h$, it can be concluded that $G^* \subseteq \bigcap_{h \in H} X_h$. Furthermore, if \tilde{Y} does not possess any causal relationships with G^* , $G^* = \bigcap_{h \in H} X_h$.

The proof can be found in **Appendix A.4**.

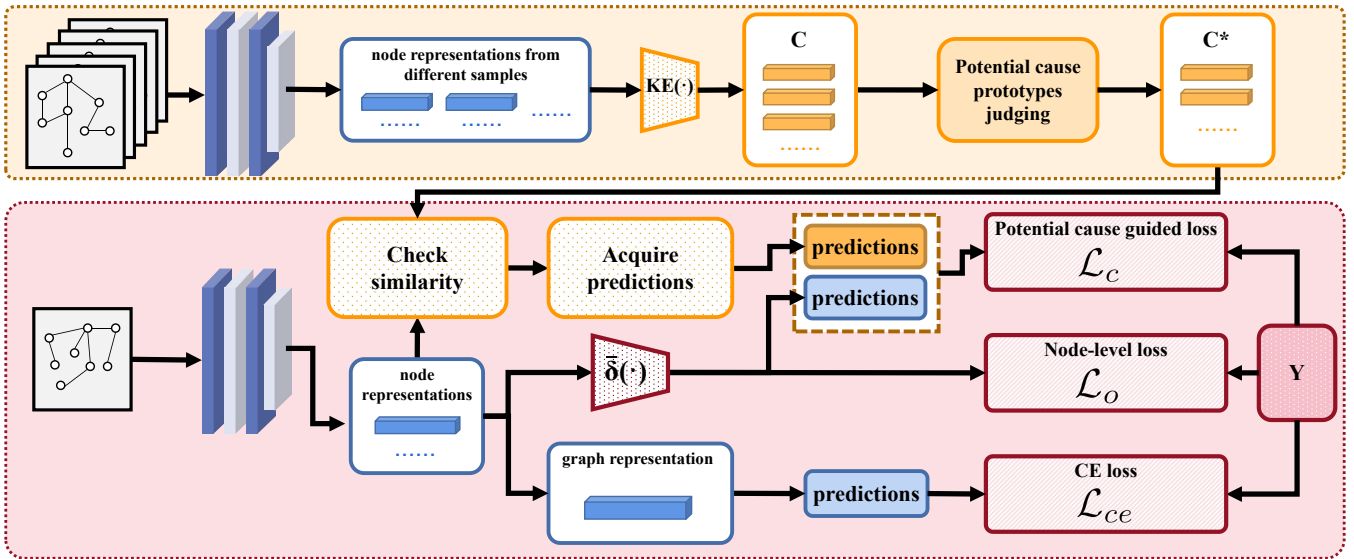


Figure 2: The framework of our proposed method. The upper yellow block delineates the process of estimating potential causes, while the lower red block illustrates the utilization of potential causes for auxiliary training.

Extracting Potential Causes.

Building upon Theorem 2, we aim to identify the potential causes of Y to construct an estimate concerning G^* . To extract potential causes from the data, it is imperative that our model possesses an elementary level of knowledge regarding the relationship between the data and labels. In pursuit of such a model, we carry out a pre-training stage for the model with μ epochs of training based on the cross-entropy loss \mathcal{L}_{ce} , where μ is a hyperparameter. For graph set $\{G_i\}_{i=1}^N$, \mathcal{L}_{ce} can be formulated as:

$$\mathcal{L}_{ce} = \sum_{i=1}^N \sum_{k=1}^K \mathcal{H}(\delta(\text{POOL}(\psi(G_i))), Y_{i,k}), \quad (3)$$

where $\mathcal{H}(\cdot)$ denotes the function that calculates the cross-entropy loss, N denotes the total number of samples. $\psi(\cdot)$ denotes the sub-network responsible for outputting node representations in GNN. $\text{POOL}(\cdot)$ conducts average pooling [Kipf and Welling, 2017] on the node representations to calculate the graph representation. $\delta(\cdot)$ projects the graph representation into label prediction.

To precisely identify potential causes at the node level, it is imperative for the GNN to explicitly model the relationship between each node and the graph label. To achieve this, we first calculate the node representations. We denote the set of all node representations corresponding to graph G_i as Z_i . Formally, we have:

$$Z_i = \psi(G_i). \quad (4)$$

Concurrently, we propose node-level loss \mathcal{L}_o to enable the model to capture the direct relationship between node representations and graph labels. \mathcal{L}_o can be formulated as:

$$\mathcal{L}_o = \sum_{i=1}^N \sum_{k=1}^K \mathcal{H}\left(\frac{1}{|\mathcal{V}_i|} \sum_{l=1}^{|\mathcal{V}_i|} \bar{\delta}(Z_{i,l}), Y_{i,k}\right), \quad (5)$$

$|\mathcal{V}_i|$ denotes the number of node within G_i , $\bar{\delta}(\cdot)$ predicts the graph label based on individual node features. $\bar{\delta}(\cdot)$ consists of a sigmoid function to project the output into $[0, 1]$. $Z_{i,l}$ denotes the l -th node representation of graph G_i calculated with $\psi(\cdot)$. We then sum up \mathcal{L}_o and \mathcal{L}_{ce} as the total loss for pretraining.

After μ epochs of pretraining, the node representations output by the GNN now embody semantic information about graph data. Subsequently, we construct a series of prototypes to encapsulate and summarize these representations. We then seek to identify potential causes from these prototypes.

Specifically, in the $(\mu + 1)$ -th epoch, we gather all output node representations $\{Z_i\}_{i=1}^N$ from all graph samples. These representations are then detached from the back-propagation process. Subsequently, we perform clustering operations on $\{Z_i\}_{i=1}^N$. The clustering process can be formulated as follows:

$$C = \text{KE}\left(\bigcap_{i \in [1, N]} Z_i\right), \quad (6)$$

where $\text{KE}(\cdot)$ denotes the data categorizing operation with K-Means and Elbow algorithms, the detailed implementation can be found in **Appendix B.1**. $\bigcap_{i \in [1, N]} Z_i$ denotes the intersection of all collected Z_i . C denotes the set of centers of grouped representations, each $c_j \in C$ denotes a prototype vector that represents the center of the j -th group.

Subsequently, we assess the qualification of c_j as a potential cause based on Definition 1. In accordance with the first condition of Definition 1, our initial evaluation investigates the dependence between c_j and Y across all contexts. Let the value space of Y be denoted as $\mathcal{D} = \{1, 2, \dots, D\}$. Instead of directly assessing the dependency, we assess that if c_j holds dependence with the event $Y = d$ across all contexts upon the satisfaction of the following conditions:

$$\bar{\delta}(Z_{i,l})_{[d]} > 1 - \Delta, \forall [i, l] \in \mathbf{W}^j, \quad (7)$$

or

$$\bar{\delta}(\mathbf{Z}_{i,l})_{[d]} < \Delta, \forall [i, l] \in \mathbf{W}^j, \quad (8)$$

where $\bar{\delta}(\mathbf{Z}_{i,l})_{[d]}$ denotes the d -th element of the vector $\bar{\delta}(\mathbf{Z}_{i,l})$, $\bar{\delta}(\mathbf{Z}_{i,l})_{[d]}$ represent the model’s judging based on node representation $\mathbf{Z}_{i,l}$ of the possibility of the graph sample belong to class d . $[i, l]$ denote the indexes. \mathbf{W}^j denotes the set of indexes of node representations that are clustered to the group with center \mathbf{c}_j . Δ is a hyperparameter. The intuition of such a design is that if the occurrence of \mathbf{c}_j does hold dependence with the event $Y = d$, then according to the designation of $\bar{\delta}(\cdot)$, $\bar{\delta}(\mathbf{Z}_{i,l})$ with $[i, l] \in \mathbf{W}^j$ will hold significant and consistent influence upon the model’s final judgment of $Y = d$. Therefore, we could sort out the potential causes by judging whether $\bar{\delta}(\cdot)$ holds a positive influence, i.e., $\bar{\delta}(\mathbf{Z}_{i,l})_{[d]} > 1 - \Delta$, or negative influence, i.e., $\bar{\delta}(\mathbf{Z}_{i,l})_{[d]} < \Delta$. If $\bar{\delta}(\cdot)$ holds neither positive influence nor negative influence, then we assert that the corresponding prototype is not a potential cause.

Next, we assess if the second condition of Definition 1 holds. According to the second condition, if \mathbf{c}_j is a potential cause, there needs to exist an extra factor that is independent with \mathbf{c}_j and dependent with Y . In the context of graph representation learning, fulfilling this condition is easily achievable. Since graph data comprises a wealth of complex information, we assume that such extra factors always exist, as long as the number of prototypes we discover exceeds ξ , ξ is a hyperparameter. Otherwise, we skip the training for this round.

The final selected prototypes \mathbf{c}_j^* consist the set C^* . C^* will be utilized for the downstream training.

Auxiliary Training.

Up to this point, we have identified all potential causes that meet the specified criteria. However, it is challenging to seamlessly map these prototypes back to the graph data, rendering direct utilization in GNN training impractical. Consequently, we have devised an auxiliary training procedure to integrate the potential causes and guide the model training process.

According to Theorem 1 and Corollary 2, we could train a GNN model to achieve the theoretically best performance even under a PLL scenario with G^* and the loss function defined in Equation 2. Furthermore, according to Theorem 2, we could adopt the potential causes to replace G^* to a certain extent. Therefore, we opt to find the correlation between the prototypes C^* that are judged to be potential causes and Y , then utilize C^* for guidance for GNN training. Specifically, we directly adopt a vector \mathbf{o}_j as the prediction of graph labels based on \mathbf{c}_j . $\mathbf{o}_j \in \mathbb{R}^{1 \times D}$. \mathbf{o}_j is initialized with the value of $\bar{\delta}(\mathbf{c}_j^*)$ from $(\mu + 1)$ -th epoch, and set as a trainable vector. \mathbf{o}_j is updated using the following loss function:

$$\mathcal{L}_v = \sum_{i=1}^N \sum_{k=1}^K \mathcal{H}\left(e^{\left(\frac{1}{|\mathcal{V}_i|} \sum_{l=1}^{|\mathcal{V}_i|} w_{i,l}\right)^\lambda}, Y_{i,k}\right), \quad (9)$$

where $w_{i,l}$ is the l -th node-level prediction vector according to the l -th node representation within the i -th sample. $w_{i,l}$

can be calculated with the following equation:

$$w_{i,l} = \begin{cases} \mathbf{o}_j, & \text{if } \mathbf{Z}_{i,l} \text{ is most similar to } \mathbf{c}_j^* \\ 0, & \text{if } \mathbf{Z}_{i,l} \text{ is not similar to any } \mathbf{c}_j^* \in C^* \end{cases} \quad (10)$$

The similarity judgment principle is given in Appendix B.2. Then, we leverage predictions made based on potential causes to guide our training process. Specifically, we propose the following loss function:

$$\mathcal{L}_g = \sum_{i=1}^N \mathcal{H}\left(\frac{1}{|\mathcal{V}_i|} \sum_{l=1}^{|\mathcal{V}_i|} w_{i,l}, h(g(G_i))\right), \quad (11)$$

The total loss \mathcal{L}_c for potential cause guided learning can be formulated as:

$$\mathcal{L}_c = \mathcal{L}_g + \mathcal{L}_v. \quad (12)$$

Furthermore, \mathcal{L}_o in Equation 5 is also included in our training objective, allowing us to update $\delta(\cdot)$ and $g(\cdot)$ during the training process. Simultaneously, we also train the model with CE loss \mathcal{L}_{ce} defined in Equation 3. \mathcal{L}_c , \mathcal{L}_{ce} , and \mathcal{L}_o are summed up to update our model. We update our model for $\lfloor \frac{u}{2} \rfloor$ epochs and relocate the potential causes, until convergence or reach maximum epochs.

4 Experiments

4.1 Comparison with State-of-the-art methods

Datasets.

We conducted experiments on seven widely employed graph datasets: Graph-SST5 [Yuan *et al.*, 2023], Graph-SST5 (OOD) [Yuan *et al.*, 2023; Wu *et al.*, 2022b], Graph-Twitter [Yuan *et al.*, 2023], Graph-Twitter (OOD) [Yuan *et al.*, 2023; Wu *et al.*, 2022b], Graph-SST2 [Yuan *et al.*, 2023], COLLAB [Kersting *et al.*, 2016], and REDDIT-MULTI-5K [Kersting *et al.*, 2016]. Detailed information about these datasets is provided in Appendix C.1. Using these datasets, we introduced two types of label noise: random label noise, where we added randomly selected labels to the original dataset, and competitive label noise, where we introduced a label strongly correlated with the ground-truth label to induce confusion. Specifically, for competitive label noise, we construct datasets with different label ambiguity levels ρ . Please refer to Appendix C.2. for details.

Settings.

We compare GPCD with six baseline methods, including 1) graph causal learning methods: DIR [Wu *et al.*, 2022b], CIGA [Chen *et al.*, 2022], DISC [Fan *et al.*, 2022c]; 2) PLL methods: PICO [Wang *et al.*, 2022a], ML-PLL [Yan and Guo, 2023]; 3) conventional GNN method ARMA [Bianchi *et al.*, 2022]. To ensure a fair comparison, we employed the same GNN backbone and dataset settings for all methods. Please refer to Appendix C.3 for details. To validate the effectiveness of \mathcal{L}_v and auxiliary training, we conducted two ablation experiments. For GPCD-w/o- λ , we set the λ value to 1, and the function’s concavity was removed according to Theorem 1. For GPCD-w/o-auxiliary, we eliminated the extraction of potential causes, and potential causes were no longer utilized as auxiliary during the training process.

Table 1: Comparison of test accuracy (mean \pm std) across seven datasets under random label noise. Best records are highlighted in **bold**, while second-best records are marked with underline.

Method	Graph-SST5 (OOD)	Graph-SST5 (ID)	Graph-Twitter (OOD)	Graph-Twitter (ID)	Graph-SST2	COLLAB	REDDIT-MULTI-5K
ARMA [Bianchi et al., 2022]	35.43 \pm 1.19	44.83 \pm 2.84	54.00 \pm 4.00	55.52 \pm 3.90	83.63 \pm 1.58	63.33 \pm 2.84	40.32 \pm 4.99
DIR [Wu et al., 2022b]	33.95 \pm 4.60	33.75 \pm 5.72	47.48 \pm 6.31	48.17 \pm 3.95	44.10 \pm 0.01	53.57 \pm 3.52	37.33 \pm 4.62
CIGA [Chen et al., 2022]	38.28 \pm 4.07	45.66 \pm 0.87	61.64 \pm 2.90	60.14 \pm 1.68	85.02 \pm 0.69	61.20 \pm 2.80	39.82 \pm 1.92
DISC [Fan et al., 2022b]	37.70 \pm 0.10	35.81 \pm 0.10	53.00 \pm 2.03	56.04 \pm 0.36	83.41 \pm 4.50	57.33 \pm 0.23	42.11 \pm 3.12
PiCO [Wang et al., 2022a]	39.69 \pm 3.65	45.84 \pm 0.93	60.17 \pm 0.22	51.14 \pm 0.67	30.89 \pm 0.36	48.34 \pm 0.12	35.05 \pm 0.59
ML-PLL [Yan and Guo, 2023]	32.22 \pm 1.96	42.69 \pm 0.30	42.60 \pm 0.35	51.12 \pm 2.97	87.29\pm1.07	51.87 \pm 3.35	36.66 \pm 0.42
GPCD-w/o- λ	42.37 \pm 1.74	47.37 \pm 0.21	62.67 \pm 0.13	61.05 \pm 0.07	86.20 \pm 0.10	64.07 \pm 1.10	45.51 \pm 0.57
GPCD-w/o-auxiliary	42.31 \pm 0.57	47.33 \pm 0.24	61.81 \pm 0.27	60.61 \pm 0.08	86.86 \pm 0.19	63.67 \pm 0.31	45.18 \pm 0.31
GPCD	44.69\pm2.11	48.01\pm0.18	63.97\pm1.33	61.29\pm0.08	87.12 \pm 0.16	65.07\pm0.23	49.10\pm0.35

Table 2: Test accuracy (mean \pm std) comparison on three datasets with competitive label noise at different ambiguity levels ρ . The label semantically closest to the ground-truth is added to the candidate label set with a probability of ρ . Best records are highlighted in **bold**, while second-best records are marked with underline.

Method	Graph-SST5 ($\rho = 0.9$)	Graph-Twitter ($\rho = 0.9$)	COLLAB ($\rho = 0.9$)	Graph-SST5 ($\rho = 0.7$)	Graph-Twitter ($\rho = 0.7$)	COLLAB ($\rho = 0.7$)
ARMA [Bianchi et al., 2022]	39.83 \pm 0.70	46.69 \pm 0.88	60.27 \pm 3.72	42.64 \pm 0.65	47.41 \pm 5.20	59.67 \pm 0.07
DIR [Wu et al., 2022b]	38.98 \pm 0.30	45.15 \pm 1.16	57.10 \pm 0.17	38.95 \pm 1.77	44.19 \pm 5.70	50.17 \pm 1.15
CIGA [Chen et al., 2022]	41.65 \pm 1.32	57.22 \pm 1.34	<u>60.35\pm2.22</u>	42.64 \pm 1.48	60.28 \pm 1.75	60.72 \pm 3.69
DISC [Fan et al., 2022c]	39.38 \pm 0.12	52.31 \pm 0.57	50.20 \pm 0.05	38.95 \pm 2.48	54.32 \pm 3.24	54.13 \pm 0.23
PiCO [Wang et al., 2022a]	41.93 \pm 0.19	57.83 \pm 0.56	49.80 \pm 1.13	43.65 \pm 0.86	55.79 \pm 0.64	37.09 \pm 1.78
ML-PLL [Yan and Guo, 2023]	42.30 \pm 0.26	51.20 \pm 0.03	46.80 \pm 0.57	42.86 \pm 0.34	51.12 \pm 2.97	52.64 \pm 2.59
GPCD-w/o- λ	<u>42.72\pm0.08</u>	57.25 \pm 0.18	60.33 \pm 0.28	43.48 \pm 0.13	<u>61.19\pm0.22</u>	60.60 \pm 0.57
GPCD-w/o-auxiliary	42.19 \pm 0.15	57.16 \pm 0.38	60.01 \pm 0.59	45.31 \pm 0.30	59.46 \pm 0.08	61.53 \pm 0.81
GPCD	43.03\pm0.29	58.69\pm0.07	61.52\pm0.97	46.54\pm0.66	61.31\pm0.18	63.73\pm1.01

Results.

Experimental results are reported in Table 1 and 2. From the results, it can be observed that GPCD has generally outperformed all the baseline methods. On OOD data, GPCD still demonstrates strong generalization performance. Even under competitive label noise, GPCD continues to exhibit excellent performance. In the ablation experiments, GPCD’s performance was superior to GPCD-w/o- λ and GPCD-w/o-auxiliary, demonstrating the effectiveness of our designs. The experimental results indicate that GPCD has successfully extracted meaningful potential causes and these causes positively impact the training process.

4.2 In-depth Study

Analysis on Causality of Representations.

In Figure 3, we visualize the dimension of the node-level prediction vector that matches the correct ground-truth class of the Graph-Twitter dataset, which can demonstrate our model relay on which words to make the final prediction. In Figure 3, we visualize the element in the dimension of the node-level prediction vector aligned with the correct class within the Graph-Twitter dataset, illustrating the reliance of our model on specific words for making final predictions. As depicted in Figure 3(a), (b), and (c), words like “damn” and “hate” for negativity, “vs” for neutrality, and “love” for positivity exhibit strong relevance with their corresponding ground-truth labels. Moreover, GPCD effectively captures the intrinsic semantics of sentences within the test set. In Figure 3(d), (e), and

(f), it emphasizes words such as “hate”, “worse”, “WorldOfWouter”, and “awesome”, all conveying sentiment. This underscores GPCD’s ability to capture pivotal sentiment-related vocabulary, leading to enhanced accuracy in sentiment classification for the partial-label dataset.

Visualization Study.

As shown in Figure 4, we visualize the graph feature obtained on the Graph-Twitter dataset with random label noise using t-SNE [Van der Maaten and Hinton, 2008]. Specifically, we visualize the features acquired by the three methods: a) ARMA: a model using ARMA backbone that treats each label equally; b) PICO: a partial-label method that excels in feature learning; c) Our method GPCD.

As observed in the figure, the features obtained by ARMA from different categories are mixed together in the feature space. Although PICO separates the features into three clusters on the training set, the categories within each cluster are still mixed. In addition, the features obtained by PICO lack generalization, as their distributions on the training and test sets are entirely different. On the contrary, GPCD’s features on the training set are clustered into three groups, and they maintain the same distribution on the test set. From a causal perspective, GPCD can capture features from the topological graph that are closely related to the ground-truth label.

Training Procure Study.

In Figure 5, we conducted a comprehensive comparative analysis of the performance of various models throughout the

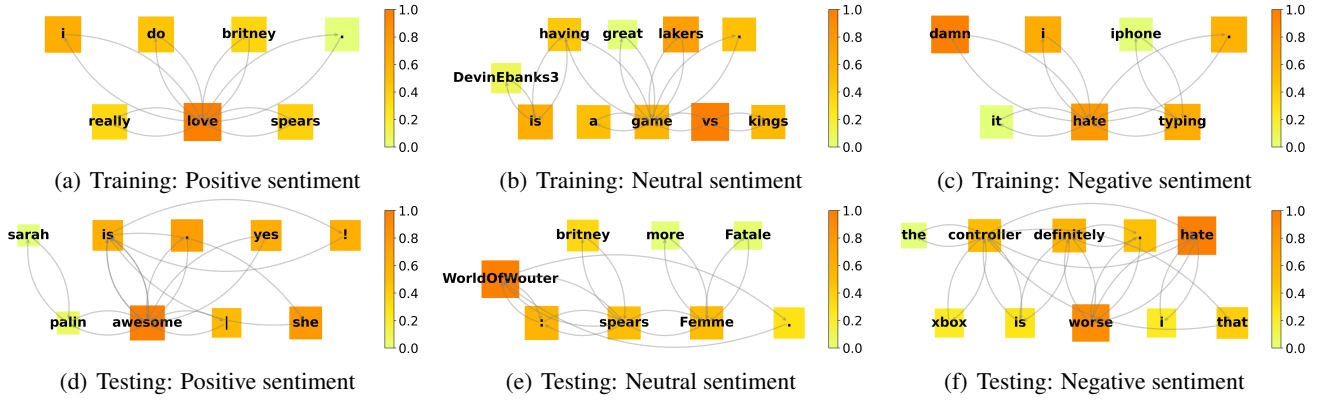


Figure 3: Visualization of the node-level prediction vector on the Graph-Twitter dataset. Each graph represents a sentence. Each node’s color intensity represents the classification probability of the node-level prediction vector on the ground-truth label.

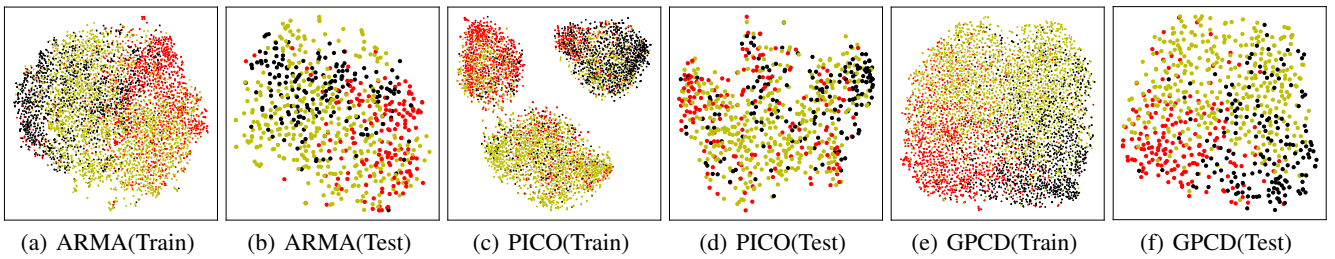


Figure 4: T-SNE visualization of the graph features on Graph-Twitter with random label noise. The first and second rows represent the features extracted from the training set and test set, respectively.

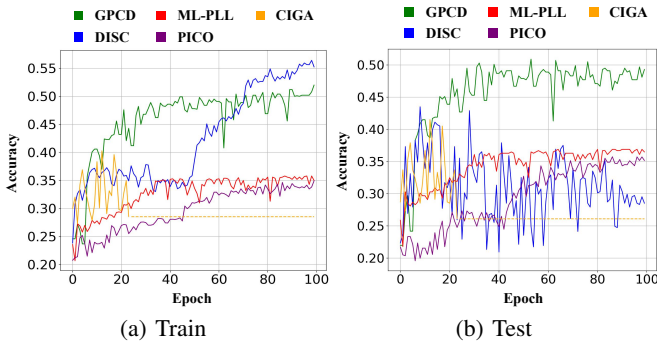


Figure 5: Comparison of GPCD’s performance on the REDDIT-MULTI-5K dataset with other methods along the training procedure.

entire training process. The results reveal that the GPCD model surpasses other models in terms of performance, exhibiting higher learning efficiency and enhanced stability. It is noteworthy that although DISC achieved better results in the subsequent learning phase on the training set, only GPCD demonstrates optimal performance on the test set. This substantiates that our method not only eliminates interference information but also consistently learns stably.

Model Structure Study.

We performed an analysis of some parameters employed in our method as a verification of the model structure, as illustrated in Figure 6(a). The results indicate that an appropriate number of pre-training epochs (μ) plays a crucial role

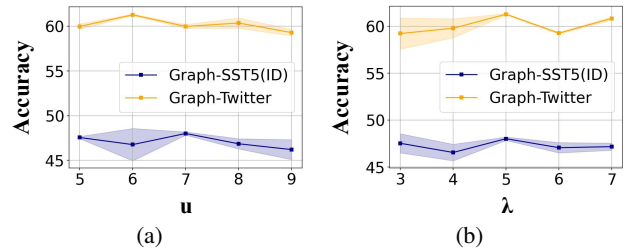


Figure 6: Performance of GPCD with different μ and λ .

in facilitating the extraction of meaningful potential causes, ultimately contributing to optimal model performance. Figure 6(b) further elucidates that a relatively larger value of the hyperparameter λ corresponds to more favorable outcomes, aligning with empirically validated research findings.

5 Conclusion

We present a novel method, GPCD, designed to facilitate the proficient acquisition of discriminative information by GNN models within the context of Partially Labeled Learning. GPCD achieves its objective by effectively mitigating label noise inherent in the data through the identification of potential causes present within the graph data. We provide a theoretical analysis to substantiate the rationale behind GPCD’s design. Furthermore, a series of empirical investigations ascertain the empirical superiority of GPCD.

References

- [Bevilacqua *et al.*, 2021] Beatrice Bevilacqua, Yangze Zhou, and Bruno Ribeiro. Size-invariant graph representations for graph classification extrapolations. In Marina Meila and Tong Zhang, editors, *Proceedings of the 38th International Conference on Machine Learning, ICML 2021, 18-24 July 2021, Virtual Event*, volume 139 of *Proceedings of Machine Learning Research*, pages 837–851. PMLR, 2021.
- [Bianchi *et al.*, 2022] Filippo Maria Bianchi, Daniele Grattarola, Lorenzo Livi, and Cesare Alippi. Graph neural networks with convolutional ARMA filters. *IEEE Trans. Pattern Anal. Mach. Intell.*, 44(7):3496–3507, 2022.
- [Chai *et al.*, 2019] Jing Chai, Ivor W Tsang, and Weijie Chen. Large margin partial label machine. *IEEE Transactions on Neural Networks and Learning Systems*, 31(7):2594–2608, 2019.
- [Chang *et al.*, 2020] Shiyu Chang, Yang Zhang, Mo Yu, and Tommi S. Jaakkola. Invariant rationalization. In *Proceedings of the 37th International Conference on Machine Learning, ICML 2020, 13-18 July 2020, Virtual Event*, volume 119 of *Proceedings of Machine Learning Research*, pages 1448–1458. PMLR, 2020.
- [Chen *et al.*, 2022] Yongqiang Chen, Yonggang Zhang, Yatao Bian, Han Yang, Kaili Ma, Binghui Xie, Tongliang Liu, Bo Han, and James Cheng. Learning causally invariant representations for out-of-distribution generalization on graphs. In *NeurIPS*, 2022.
- [Cour *et al.*, 2011] Timothee Cour, Ben Sapp, and Ben Taskar. Learning from partial labels. *The Journal of Machine Learning Research*, 12:1501–1536, 2011.
- [Dutta, 2001] Amitava Dutta. Telecommunications and economic activity: An analysis of granger causality. *J. Manag. Inf. Syst.*, 17(4):71–96, 2001.
- [Fan *et al.*, 2022a] Shaohua Fan, Xiao Wang, Yanhu Mo, Chuan Shi, and Jian Tang. Debiasing graph neural networks via learning disentangled causal substructure. In *NeurIPS*, 2022.
- [Fan *et al.*, 2022b] Shaohua Fan, Xiao Wang, Yanhu Mo, Chuan Shi, and Jian Tang. Debiasing graph neural networks via learning disentangled causal substructure. *Advances in Neural Information Processing Systems*, 35:24934–24946, 2022.
- [Fan *et al.*, 2022c] Shaohua Fan, Xiao Wang, Yanhu Mo, Chuan Shi, and Jian Tang. Debiasing graph neural networks via learning disentangled causal substructure. In Sanmi Koyejo, S. Mohamed, A. Agarwal, Danielle Belgrave, K. Cho, and A. Oh, editors, *Advances in Neural Information Processing Systems 35: Annual Conference on Neural Information Processing Systems 2022, NeurIPS 2022, New Orleans, LA, USA, November 28 - December 9, 2022*, 2022.
- [Gong *et al.*, 2022] Xiuwen Gong, Dong Yuan, and Wei Bao. Partial label learning via label influence function. In Kamalika Chaudhuri, Stefanie Jegelka, Le Song, Csaba Szepesvári, Gang Niu, and Sivan Sabato, editors, *International Conference on Machine Learning, ICML 2022, 17-23 July 2022, Baltimore, Maryland, USA*, volume 162 of *Proceedings of Machine Learning Research*, pages 7665–7678. PMLR, 2022.
- [Guo *et al.*, 2021] Ruocheng Guo, Lu Cheng, Jundong Li, P. Richard Hahn, and Huan Liu. A survey of learning causality with data: Problems and methods. *ACM Comput. Surv.*, 53(4):75:1–75:37, 2021.
- [He *et al.*, 2020] Kaiming He, Haoqi Fan, Yuxin Wu, Saining Xie, and Ross B. Girshick. Momentum contrast for unsupervised visual representation learning. In *2020 IEEE/CVF Conference on Computer Vision and Pattern Recognition, CVPR 2020, Seattle, WA, USA, June 13-19, 2020*, pages 9726–9735. Computer Vision Foundation / IEEE, 2020.
- [Hüllermeier and Beringer, 2006] Eyke Hüllermeier and Jürgen Beringer. Learning from ambiguously labeled examples. *Intelligent Data Analysis*, 10(5):419–439, 2006.
- [Jiao *et al.*, 2023] Licheng Jiao, Jie Chen, Fang Liu, Shuyuan Yang, Chao You, Xu Liu, Lingling Li, and Biao Hou. Graph representation learning meets computer vision: A survey. *IEEE Trans. Artif. Intell.*, 4(1):2–22, 2023.
- [Jin and Ghahramani, 2002] Rong Jin and Zoubin Ghahramani. Learning with multiple labels. *Advances in neural information processing systems*, 15, 2002.
- [Kersting *et al.*, 2016] Kristian Kersting, Nils M. Kriege, Christopher Morris, Petra Mutzel, and Marion Neumann. Benchmark data sets for graph kernels, 2016. <http://graphkernels.cs.tu-dortmund.de>.
- [Kipf and Welling, 2017] Thomas N. Kipf and Max Welling. Semi-supervised classification with graph convolutional networks. In *5th International Conference on Learning Representations, ICLR 2017, Toulon, France, April 24-26, 2017, Conference Track Proceedings*. OpenReview.net, 2017.
- [Lee *et al.*, 2019] Junhyun Lee, Inyeop Lee, and Jaewoo Kang. Self-attention graph pooling. In *International conference on machine learning*, pages 3734–3743. PMLR, 2019.
- [Liu and Dietterich, 2012] Liping Liu and Thomas Dietterich. A conditional multinomial mixture model for superset label learning. *Advances in neural information processing systems*, 25, 2012.
- [Nguyen and Caruana, 2008] Nam Nguyen and Rich Caruana. Classification with partial labels. In *Proceedings of the 14th ACM SIGKDD international conference on Knowledge discovery and data mining*, pages 551–559, 2008.
- [Nguyen and Grishman, 2018] Thien Huu Nguyen and Ralph Grishman. Graph convolutional networks with argument-aware pooling for event detection. In Sheila A. McIlraith and Kilian Q. Weinberger, editors, *Proceedings of the Thirty-Second AAAI Conference on Artificial*

- Intelligence, (AAAI-18), New Orleans, Louisiana, USA, February 2-7, 2018, pages 5900–5907. AAAI Press, 2018.*
- [Pearl and others, 2000] Judea Pearl et al. Models, reasoning and inference. *Cambridge, UK: Cambridge University Press*, 19(2):3, 2000.
- [Pikhurko and Verbitsky, 2009] Oleg Pikhurko and Oleg Verbitsky. Logical complexity of graphs: A survey. In Martin Grohe and Johann A. Makowsky, editors, *Model Theoretic Methods in Finite Combinatorics - AMS-ASL Joint Special Session, Washington, DC, USA, January 5-8, 2009*, volume 558 of *Contemporary Mathematics*, pages 129–180. American Mathematical Society, 2009.
- [Shamsi et al., 2022] Kiarash Shamsi, Friedhelm Victor, Murat Kantarcioglu, Yulia R. Gel, and Cuneyt Gurcan Akcora. Chartalist: Labeled graph datasets for UTXO and account-based blockchains. In *NeurIPS*, 2022.
- [Shen et al., 2023] Yinghan Shen, Xuhui Jiang, Zijian Li, Yuanzhuo Wang, Chengjin Xu, Huawei Shen, and Xueqi Cheng. Uniskg: A unified representation learning framework of social network and knowledge graph. *Neural Networks*, 158:142–153, 2023.
- [Szummer, 2002] Marcin Szummer. *Learning from partially labeled data*. PhD thesis, Massachusetts Institute of Technology, Cambridge, MA, USA, 2002.
- [Van der Maaten and Hinton, 2008] Laurens Van der Maaten and Geoffrey Hinton. Visualizing data using t-sne. *Journal of machine learning research*, 9(11), 2008.
- [Vaswani et al., 2017] Ashish Vaswani, Noam Shazeer, Niki Parmar, Jakob Uszkoreit, Llion Jones, Aidan N. Gomez, Lukasz Kaiser, and Illia Polosukhin. Attention is all you need. In Isabelle Guyon, Ulrike von Luxburg, Samy Bengio, Hanna M. Wallach, Rob Fergus, S. V. N. Vishwanathan, and Roman Garnett, editors, *Advances in Neural Information Processing Systems 30: Annual Conference on Neural Information Processing Systems 2017, December 4-9, 2017, Long Beach, CA, USA*, pages 5998–6008, 2017.
- [Velickovic et al., 2017] Petar Velickovic, Guillem Cucurull, Arantxa Casanova, Adriana Romero, Pietro Lio, Yoshua Bengio, et al. Graph attention networks. *stat*, 1050(20):10–48550, 2017.
- [Wang et al., 2022a] Haobo Wang, Ruixuan Xiao, Yixuan Li, Lei Feng, Gang Niu, Gang Chen, and Junbo Zhao. Pico: Contrastive label disambiguation for partial label learning. In *The Tenth International Conference on Learning Representations, ICLR 2022, Virtual Event, April 25-29, 2022*. OpenReview.net, 2022.
- [Wang et al., 2022b] Yifan Wang, Yiping Song, Shuai Li, Chaoran Cheng, Wei Ju, Ming Zhang, and Sheng Wang. Disencite: Graph-based disentangled representation learning for context-specific citation generation. In *Thirty-Sixth AAAI Conference on Artificial Intelligence, AAAI 2022, Thirty-Fourth Conference on Innovative Applications of Artificial Intelligence, IAAI 2022, The Twelfth Symposium on Educational Advances in Artificial Intelligence, EAAI 2022 Virtual Event, February 22 - March 1, 2022*, pages 11449–11458. AAAI Press, 2022.
- [Wu et al., 2022a] Junran Wu, Xueyuan Chen, Ke Xu, and Shangzhe Li. Structural entropy guided graph hierarchical pooling. In Kamalika Chaudhuri, Stefanie Jegelka, Le Song, Csaba Szepesvári, Gang Niu, and Sivan Sabato, editors, *International Conference on Machine Learning, ICML 2022, 17-23 July 2022, Baltimore, Maryland, USA*, volume 162 of *Proceedings of Machine Learning Research*, pages 24017–24030. PMLR, 2022.
- [Wu et al., 2022b] Yingxin Wu, Xiang Wang, An Zhang, Xiangan He, and Tat-Seng Chua. Discovering invariant rationales for graph neural networks. In *The Tenth International Conference on Learning Representations, ICLR 2022, Virtual Event, April 25-29, 2022*. OpenReview.net, 2022.
- [Xia et al., 2021] Feng Xia, Ke Sun, Shuo Yu, Abdul Aziz, Liangtian Wan, Shirui Pan, and Huan Liu. Graph learning: A survey. *IEEE Trans. Artif. Intell.*, 2(2):109–127, 2021.
- [Yan and Guo, 2023] Yan Yan and Yuhong Guo. Mutual partial label learning with competitive label noise. In *The Eleventh International Conference on Learning Representations, ICLR 2023, Kigali, Rwanda, May 1-5, 2023*. OpenReview.net, 2023.
- [Ying et al., 2019] Zhitao Ying, Dylan Bourgeois, Jiaxuan You, Marinka Zitnik, and Jure Leskovec. Gnnexplainer: Generating explanations for graph neural networks. *Advances in neural information processing systems*, 32, 2019.
- [You et al., 2020] Yuning You, Tianlong Chen, Yongduo Sui, Ting Chen, Zhangyang Wang, and Yang Shen. Graph contrastive learning with augmentations. In Hugo Larochelle, Marc’Aurelio Ranzato, Raia Hadsell, Maria-Florina Balcan, and Hsuan-Tien Lin, editors, *Advances in Neural Information Processing Systems 33: Annual Conference on Neural Information Processing Systems 2020, NeurIPS 2020, December 6-12, 2020, virtual*, 2020.
- [Yu and Zhang, 2016] Fei Yu and Min-Ling Zhang. Maximum margin partial label learning. In *Asian conference on machine learning*, pages 96–111. PMLR, 2016.
- [Yuan et al., 2023] Hao Yuan, Haiyang Yu, Shurui Gui, and Shuiwang Ji. Explainability in graph neural networks: A taxonomic survey. *IEEE Trans. Pattern Anal. Mach. Intell.*, 45(5):5782–5799, 2023.
- [Zhang and Yu, 2015] Min-Ling Zhang and Fei Yu. Solving the partial label learning problem: An instance-based approach. In Qiang Yang and Michael J. Wooldridge, editors, *Proceedings of the Twenty-Fourth International Joint Conference on Artificial Intelligence, IJCAI 2015, Buenos Aires, Argentina, July 25-31, 2015*, pages 4048–4054. AAAI Press, 2015.
- [Zhang et al., 2022] Xiwen Zhang, Weiwen Wang, Chuan-Xian Ren, and Dao-Qing Dai. Learning representation for multiple biological networks via a robust graph regularized integration approach. *Briefings Bioinform.*, 23(1), 2022.

A Proofs

A.1 Proof of Corollary 1

If G is causally redundant, according to Definition 2, we only need to remove all \tilde{G} that satisfied Equation 1 to acquire G^* . Apparently, such G^* satisfied $f_{\theta^*}(G) = f_{\theta^*}(G^*)$.

Furthermore, as all \tilde{G} that satisfying Equation 1 are removed, we have:

$$f_{\theta^*}(G^*) \neq f_{\theta^*}(G^* \setminus \tilde{G}), \forall \tilde{G} \neq \emptyset. \quad (13)$$

As f_{θ^*} accurately captures the causal relationship between G and the corresponding label Y , and can always output the correct prediction given any input.

According to the definition of mutual information, we have:

$$I(f_{\theta^*}(G^*); Y) = H(Y). \quad (14)$$

And:

$$I(f_{\theta^*}(G^* \setminus \tilde{G}); Y) = H(Y) - H(Y|f_{\theta^*}(G^* \setminus \tilde{G})). \quad (15)$$

Based on the property of entropy, we have:

$$H(Y|f_{\theta^*}(G^* \setminus \tilde{G})) \geq 0. \quad (16)$$

Furthermore, if:

$$H(Y|f_{\theta^*}(G^* \setminus \tilde{G})) = 0, \quad (17)$$

then the value of Y can be fully decided with $f_{\theta^*}(G^* \setminus \tilde{G})$, which means that G^* is causally redundant, which is in controversy with the given definition of G^* . Then, we can get the following:

$$I(f_{\theta^*}(G^*); Y) > I(f_{\theta^*}(G^* \setminus \tilde{G}); Y), \forall \tilde{G} \neq \emptyset \text{ and } \tilde{G} \in G^*. \quad (18)$$

The corollary is proofed.

A.2 Proof of Theorem 1

To prove the theorem, we first demonstrate that the value of θ actually equals the value of θ^* in Definition 2. According to Theorem 1, \mathcal{L} reaches its minimal value. \mathcal{L} can be formulated as follows:

$$\begin{aligned} \mathcal{L} &= \sum_{i=0}^N H(Y_i^*, e^{(f_{\theta}(G_i^*))^\lambda}) + \sum_{i=0}^N H(\tilde{Y}_i, e^{(f_{\theta}(G_i^*))^\lambda}) \\ &= - \sum_{i=0}^N Y_i^* \log(e^{(f_{\theta}(G_i^*))^\lambda}) - \sum_{i=0}^N \tilde{Y}_i \log(e^{(f_{\theta}(G_i^*))^\lambda}) \\ &= - \sum_{i=0}^N Y_i^* (f_{\theta}(G_i^*))^\lambda - \sum_{i=0}^N \tilde{Y}_i (f_{\theta}(G_i^*))^\lambda. \end{aligned} \quad (19)$$

As Y_i^* and \tilde{Y}_i are one-hot vectors, Equation 19 can be formulated as:

$$\mathcal{L} = - \sum_{i=0}^N (X_{i,k^*})^\lambda - \sum_{i=0}^N (X_{i,\tilde{k}})^\lambda, \quad (20)$$

where X_i denote the output of $f_{\theta}(\cdot)$ with G_i^* as the input. X_{i,k^*} denote k^* -th dimension of X_i , $Y_{i,k^*}^* = 1$. Likewise, $X_{i,\tilde{k}}$ denote \tilde{k} -th dimension of X_i , $\tilde{Y}_{i,\tilde{k}} = 1$. We also have:

$$\sum_{k=0}^K X_{i,k} = 1, \forall i \in [0, n]. \quad (21)$$

According to the definition of \mathcal{L} , $\lambda > 1$, then $(X_{i,k^*})^\lambda$ is a strictly concave function of X_{i,k^*} . Therefore, with convexity inequality, we can conclude that:

$$\delta(1)^\lambda + (1-\delta)(0)^\lambda > ((1-\delta) \cdot 1 + \delta \cdot 0)^\lambda, \forall \delta \in [0, 1] \quad (22)$$

then, we have:

$$\delta(1)^\lambda + (1-\delta)(1)^\lambda > ((1-\delta) \cdot 1)^\lambda + (\delta \cdot 1)^\lambda, \forall \delta \in [0, 1] \quad (23)$$

i.e:

$$(1)^\lambda > (1-\delta)^\lambda + \delta^\lambda, \forall \delta \in [0, 1]. \quad (24)$$

From Equation 24, we can concluded that \mathcal{L} reaches minimal if and only if $X_{i,k^*} = 1, \forall i \in \{0, 1, 2, \dots, n\}$ or $X_{i,\tilde{k}} = 1, \forall i \in \{0, 1, 2, \dots, n\}$. As G^* consists of only the data that is causally related to the true labels, and the value of \tilde{Y} cannot be entirely determined solely by G^* and the ancestors of G^* , therefore the latter can only be true when $Y^* = \tilde{Y}$. Thus, when \mathcal{L} takes its minimum, we have:

$$f_{\theta}(G^*) = Y^* = f_{\theta^*}(G^*). \quad (25)$$

The theorem is proved.

A.3 Proof of Corollary 2

We can significantly increase the value of λ , and as a result, we obtain:

$$\lim_{\lambda \rightarrow \inf} \delta^\lambda = 0, 0 \leq \delta < 1. \quad (26)$$

which means by setting λ to a sufficiently large value, we can make the predictive loss for any non-one value approaches zero. The analysis from the proof of Theorem 1 indicates that at this point, the loss can only reach its minimum value when X_{i,k^*} equals Y^* . The corollary has thus been validated.

A.4 Proof of Theorem 2

In order to prove the theorem, we first demonstrate that G^* satisfies all the conditions specified in Definition 1. We begin by demonstrating that G satisfies the first condition of Definition 1.

According to Corollary 1, we have:

$$f_{\theta^*}(G^*) = Y^*, \quad (27)$$

therefore, given any other value than G^* , $G^* \not\perp Y^*$. Obviously, G^* also dependent with Y .

Furthermore, as G^* is not causally redundant, therefore for any $\tilde{G} \subset G^*$ and $\tilde{G} \neq \emptyset$, we have $\tilde{G} \not\perp Y^*$. And, regardless of fixing the value of any element in G , $\tilde{G} \not\perp Y^*$ still

Table 3: Summary of datasets.

Name	Graphs#	Average Nodes#	Average Edges#	Classes#	Task Type	Metric
Graph-SST5(OOD)	10700	21.29	40.58	5	Classification	ACC
Graph-SST5(ID)	11855	19.85	37.70	5	Classification	ACC
Graph-Twitter(OOD)	6344	21.96	41.92	3	Classification	ACC
Graph-Twitter(ID)	6940	21.10	40.20	3	Classification	ACC
Graph-SST2	70042	10.20	18.40	2	Binary Classification	ACC
COLLAB	5000	74.49	2457.78	3	Classification	ACC
REDDIT-MULTI-5K	4999	508.52	594.87	5	Classification	ACC

Table 4: Summary of the backbones used in each dataset.

Name	Backbone#	Size of g (GNN)	Size of δ (MLP)	Global Pool
Graph-SST5(OOD)	ARMA	[768,256,128]	[128,5]	global mean pool
Graph-SST5(ID)	ARMA	[768,256,128]	[128,5]	global mean pool
Graph-Twitter(OOD)	ARMA	[768,256,128]	[128,3]	global mean pool
Graph-Twitter(ID)	ARMA	[768,256,128]	[128,3]	global mean pool
Graph-SST2	ARMA	[768,256,128]	[128,2]	global mean pool
COLLAB	ARMA	[768,256,128]	[128,3]	global mean pool
REDDIT-MULTI-5K	ARMA	[32,256,128]	[128,5]	global mean pool

holds; otherwise, it would violate the property of G^* being not causally redundant.

Based on the discussion above, we can conclude that regardless of fixing the value of any element in G , for any $\tilde{G} \subseteq G^*$ and $\tilde{G} \neq \emptyset$, $\tilde{G} \not\perp\!\!\!\perp Y^*$. Therefore, G^* satisfies the first condition of the Definition 1.

Secondly, we demonstrate that G^* satisfies the second condition of Definition 1.

Suppose there exists a causal structure [Pearl and others, 2000] that models the causal relationship of our problem, according to Equation 27, elements in G^* can be viewed as parents of Y . For any $X \subset G^*$, if all parents of X if fixed, and $G^* \setminus X_h$ will be independent with X , while is related with Y . Therefore, G^* satisfies the second condition of Definition 1.

So far, we have proved that G^* satisfies all the conditions specified in Definition 1. Therefore, $G^* \subseteq \bigcap_{h \in H} X_h$ holds, the first conclusion of the theorem is proved.

Next, we will prove that if \tilde{Y} does not possess any causal relationships with G^* , $G^* = \bigcap_{h \in H} X_h$. We have already demonstrated that $G^* \subseteq \bigcap_{h \in H} X_h$ holds; thus, we only need to establish that for the case when there exist no relationships between \tilde{Y} and G^* , any X_h satisfies $X_h \in G^*$.

If \tilde{Y} does not possess any causal relationships with G^* , then we can conclude that $X_h \not\perp\!\!\!\perp Y^*$ under all contexts. As X_h appear before Y^* , then Y^* won't hold any causal influence on X_h . Furthermore, X_h and Y^* are correlated under all contexts, which excludes the possibility of the existence of mediation or backdoor paths. Therefore, X_h holds causal influence on Y^* , therefore $X_h \subset G^*$. the second conclusion of the theorem is proved. So far, we have demonstrated the theorem.

B Implementation Details

B.1 Implementation of KE(\cdot)

Our objective is to partition variables and formulate sets of variables based on the affinity of node features. This entails employing the K-Means clustering technique on node embeddings Z acquired within a given batch, resulting in the creation of multiple clusters. Each cluster is representative of a distinct set of variables. Moreover, we leverage the Elbow algorithm to ascertain the optimal count of clusters to be derived. Concretely, we cease the expansion of cluster count at the point of inflection in the cumulative sum of squared errors, which signifies the point of optimal cluster count. Given the variance in node count across diverse graphs, graphs with fewer nodes naturally exhibit diminished cumulative sum of squared errors. To establish a uniform benchmark for comparison, we employ the mean squared error per node, calculated by dividing the cumulative sum of squared errors by the total node count across graphs. In our specific implementation, we introduce a hyperparameter denoting the threshold for the Average Mean Squared Error (AMSE). The clustering process concludes when the AMSE descends below this stipulated threshold.

B.2 Judging Metric

We aim to ascertain the degree of similarity between a given node representation and the centers contained within set C . This is accomplished through a process involving the normalization of both the node features and the feature centers, subsequently followed by the computation of the cosine similarity between these normalized entities. Upon exceeding a predetermined threshold, we categorize a node feature as akin to the corresponding feature center. From the array of feature centers demonstrating such similarity, we strategically identify the one exhibiting the highest resemblance to the

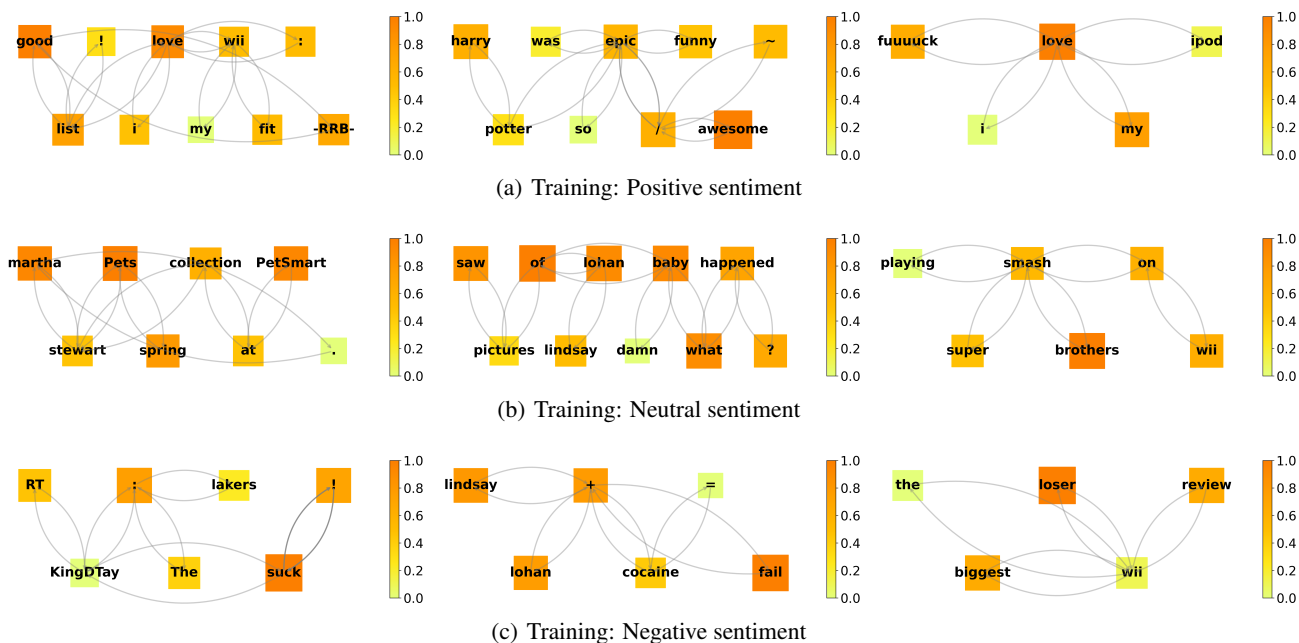


Figure 7: Visualization of node-level prediction vector on the training set of the Graph-Twitter dataset. Each graph represents a sentence.

node feature, thereby designating it for subsequent meticulous analysis. It is pertinent to underscore that the above-stated threshold is characterized as a hyperparameter, configured to optimize the performance of this process.

C Experiment

C.1 Datasets

We conducted experiments on seven widely used graph datasets: Graph-SST5 (OOD) [Yuan *et al.*, 2023; Wu *et al.*, 2022b], Graph-SST5 (ID) [Yuan *et al.*, 2023], Graph-Twitter (OOD) [Yuan *et al.*, 2023; Wu *et al.*, 2022b], Graph-Twitter (ID) [Yuan *et al.*, 2023], Graph-SST2 [Yuan *et al.*, 2023], COLLAB [Kersting *et al.*, 2016] and REDDIT-MULTI-5K [Kersting *et al.*, 2016].

(1) Graph-SST5 (OOD) dataset [Yuan *et al.*, 2023]. Graph-SST5 is a sentiment graph dataset. We follow [Wu *et al.*, 2022b] to partition the dataset into training and test sets in order to increase the task’s difficulty.

(2) Graph-SST5 (ID) dataset [Yuan *et al.*, 2023]. The original Graph-SST5 dataset.

(3) Graph-SST2 dataset [Yuan *et al.*, 2023]. Similar to the Graph-SST5 dataset, but formulated as a binary classification task.

(4) Graph-Twitter (OOD) dataset [Yuan *et al.*, 2023; Wu *et al.*, 2022b]. Similar to the Graph-SST5 dataset, but sourced from a different data origin. We follow [Wu *et al.*, 2022b] to partition the dataset into training and test sets in order to increase the task’s difficulty.

(5) Graph-Twitter (ID) dataset [Yuan *et al.*, 2023]. The original Graph-Twitter dataset.

(6) COLLAB dataset [Kersting *et al.*, 2016]. COLLAB is a scientific collaboration dataset where each graph represents

a researcher’s ego network. In this network, researchers and their collaborators are nodes, and an edge indicates a collaboration between two researchers.

(7) REDDIT-MULTI-5K dataset [Kersting *et al.*, 2016]. REDDIT-MULTI-5K is a relational dataset extracted from Reddit, with each graph representing an online discussion thread. In these graphs, users are depicted as nodes, and an edge signifies a situation where one of the two users responded to a comment made by the other user.

C.2 Create Label Noise

Two distinct forms of label noise were strategically incorporated into our study: random label noise and competitive label noise. In the context of random label noise, all erroneous labels are added to the candidate label set with the same probability. Concretely, for the binary classification Graph-SST2 dataset, an experimental framework was simulated, simulating three distinct data annotators each endowed with labeling accuracies of 100%, 70%, and 50%, respectively, reflective of their individual competencies in correctly annotating data instances. This simulation is tailored to mimic real-world complexities.

For PLL datasets with competitive label noise, a more intricate competitive label noise model was employed. This noise formulation emphasizes the augmentation of selecting labels that are semantically proximate to the ground-truth label, inherently capturing the nuances and intricacies prevalent in data. Illustratively, within the Graph-SST5 dataset, encompassing five labels encompassing various emotional tones: “very negative”, “negative”, “neutral”, “positive”, and “very positive”, a deliberate emphasis was placed on elevating the likelihood of selecting labels such as “neutral” and “very positive” when the underlying ground-truth label pertained to

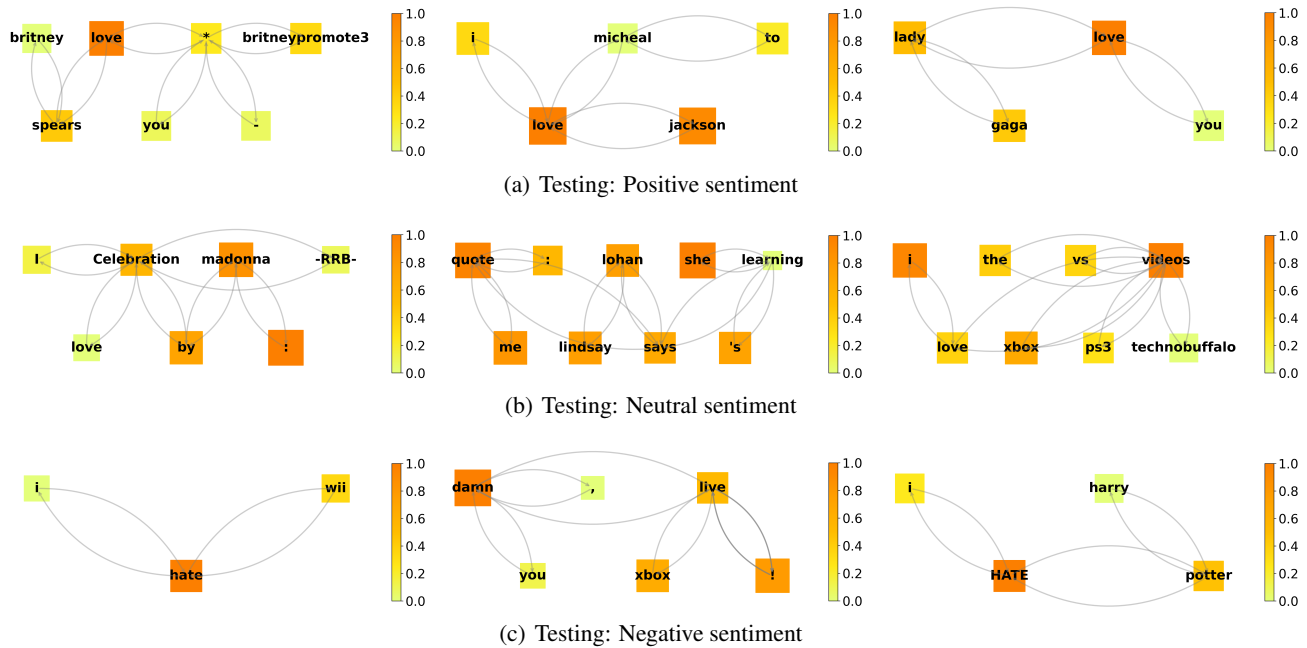


Figure 8: Visualization of node-level prediction vector on the testing set of the Graph-Twitter dataset. Each graph represents a sentence.

“positive”, thus emphasizing the thematic proximity between these concepts.

Correspondingly, the Graph-Twitter dataset similarly exhibits a tripartite labeling schema consisting of “negative”, “neutral”, and “positive” sentiments, where the contiguous labels inherently possess a heightened semantic affinity. Comparable considerations extend to the COLLAB dataset, wherein the labels “High Energy Physics”, “Condensed Matter Physics”, and “Astro Physics” are featured, with the initial two labels evincing more pronounced semantic coherence.

To introduce competitive noise, a meticulous strategy was devised: labels semantically closest to the ground-truth label are appended with a probability of ρ , thereby manifesting a salient noise component, the remaining labels are added to the candidate label set with a probability of $(1 - \rho)$, Where ρ represents the level of label ambiguity. Specifically, we constructed datasets with two levels of competitive label noise: $\rho = 0.9$ and $\rho = 0.7$.

This deliberate orchestration of competitive noise substantiates a dynamic framework that engenders heightened amalgamation of noise sources. The resultant intricacy within the noise profile enhances the evaluative capacity of our model, effectively probing its resilience in discerning discriminative patterns amidst intricate data landscapes.

C.3 Implementation Details

We compared the proposed GPCD with the following methods: 1)ML-PLL [Yan and Guo, 2023] constructs a transformation matrix to model the relationship between the candidate label set and the ground-truth label. It utilizes a mutual learning paradigm to coordinate and guide the learning of two classifiers; 2) PiCO [Wang et al., 2022a] adopts contrastive learning to enhance feature learning and employs a

strategy based on class prototypes to update the confidence of candidate labels; 3) CIGA [Chen et al., 2022] proposes an information-theoretic objective based on causality to maximize the extraction of invariant intra-class information from the subgraphs; 4) DISC [Fan et al., 2022c] proposes a disentangled GNN framework to capture the causal substructure in severe bias data; 5)ARMA [Bianchi et al., 2022] uses the most basic graph neural network and assigns equal weights to all labels.

We split datasets into 80% training, 10% validation, and 10% test sets. The test set accuracy, linked to the best-performing validation set, determined the final result. The pre-training epochs for all datasets were set to 5. The auxiliary training epochs for the dataset REDDIT-MULTI-5K were set to 50, while the rest of the datasets were set to 20. We set ξ as 5. The parameter λ was selected from $\{2,3,4,5,6,7\}$ based on the final results. The loss weights for \mathcal{L}_c , \mathcal{L}_g , and \mathcal{L}_{ce} were set to 1, 0.5, and 1, respectively. During the extraction of potential causes, clustering was stopped if the average mean squared error was less than 0.28. The initial value of hyperparameter Δ was set to 0.15, and it was increased after each extraction of latent causes to prevent the explosion of latent variables. The experiments indicate that an initially large Δ will result in the failure to extract latent causes. If Δ remains constant subsequently, latent causes will experience explosive growth, leading to deteriorated results. We set t to 4, potential causes were re-extracted every 4 epochs during the auxiliary training process. The model is trained by a standard Adam optimizer with a learning rate of 0.0001 and a batch size of 32.

All our experiments were conducted on a workstation with two Quadro RTX 5000 GPU (16 GB), one Intel Xeon E5-1650 CPU, 128GB RAM, and a Ubuntu 20.04 operating

system. For all experimental results, we conducted five independent runs and reported the mean \pm standard deviation.

C.4 Additional Experimental Results

In Figure 7 and 8, we present supplementary empirical findings concerning both the training and testing sets of the Graph-Twitter dataset. Whether applied to the training or testing partition, GPCD demonstrates a strong knack for identifying words that closely align with the true meaning of sentences. This natural ability allows the model to excel in accurately classifying various text inputs. The practical results presented here highlight GPCD’s skill in grasping the real essence of sentences in partial-label dataset.